

Title: Application of Response Surface Methodology to Laser-Induced Breakdown Spectroscopy: Influences of Hardware Configuration.

Author names and affiliations: J.S. Cowpe^{*a}, J.S. Astin^a, R.D. Pilkington^a, A.E. Hill^a, M. Longson^b, T. Robinson^b

^a Institute for Materials Research, University of Salford, Salford, M5 4WT, UK.

j.s.cowpe@pgr.salford.ac.uk

r.d.pilkington@salford.ac.uk

j.s.astin@salford.ac.uk

a.e.hill@salford.ac.uk

^b MKS Instruments UK Ltd, 2 St Georges Court, Hanover Business Park, Altrincham, Cheshire, WA14 5UA, UK.

Mark_Longson@mksinst.com

Tim_Robinson@mksinst.com

***Corresponding author:** J. S. Cowpe. j.s.cowpe@pgr.salford.ac.uk

Institute for Materials Research, Room 105 Maxwell Building, University of Salford, Salford, M5 4WT, UK. Telephone: +44-161-295-5268

Abstract: Response Surface Methodology (RSM) was employed to optimise LIBS analysis of single crystal silicon at atmospheric pressure and under vacuum conditions (pressure $\sim 10^{-6}$ mbar). Multivariate analysis software (StatGraphics 5.1) was used to design and analyse several multi-level, full factorial RSM experiments. A Quality Factor (QF) was conceived as the response parameter for the experiments, representing the quality of the LIBS spectrum captured for a given hardware configuration. The QF enabled the hardware configuration to be adjusted so that a best compromise between resolution, signal intensity and signal noise could be achieved. The effect on the QF of

simultaneously adjusting spectrometer gain, gate delay, gate width, lens position and spectrometer slit width was investigated, and the conditions yielding the best QF determined.

Keywords: LIBS, response surface methodology, silicon, optimisation, hardware.

1. Introduction

1.1 Initial comparison of LIBS under vacuum and atmospheric pressure

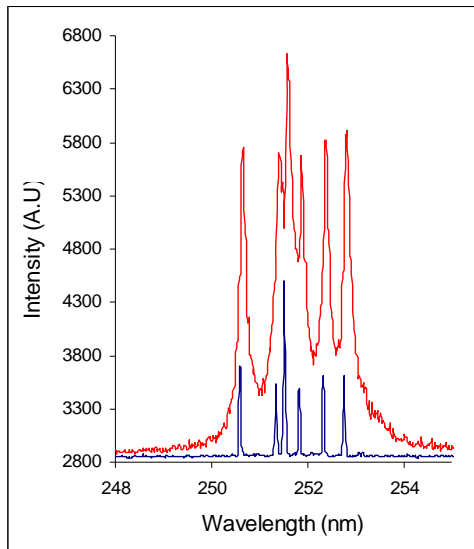


Figure 1. Comparison of LIBS spectra obtained from laser ablation of silicon at atmospheric pressure (top trace) and under vacuum conditions (bottom trace).

For a LIBS spectrum to yield useful information it must have sufficiently high resolution such that overlapping peaks may be resolved, and low background noise ensuring good sensitivity. Many hardware parameters affect the properties of the spectra obtained: laser wavelength, power, frequency and fluence, spectrometer input slit-width, ICCD gate delay and integration time, gain, focal position relative to sample, ambient atmosphere and pressure etc. Initial comparison between LIBS spectra of single crystal silicon captured at atmospheric pressure and at a pressure $\sim 10^{-6}$ mbar indicates a remarkable difference in both resolution and intensity, as shown in Figure 1. If LIBS is conducted under vacuum conditions then resolution is greatly improved [1] due to lack of pressure

broadening effects. The peak intensity [2] and the background continuum radiation are seen to diminish due to plasma expansion. Hardware optimised to produce usable spectra at atmospheric pressure no longer produces optimal spectra at lower pressures; although resolution has improved, the peak intensity has diminished.

The usual method of optimising any experimental set up is to adjust one parameter at a time, keeping all others constant, until the optimum working conditions are found. Adjusting one parameter at a time is necessarily time consuming, and may not reveal all interactions between the parameters. In order to fully describe the response and interactions of any complex system a multivariate parametric study must be conducted.

1.2 Response Surface Methodology

Response Surface Methodology (RSM) is a powerful statistical analysis technique which is well suited to modelling complex multivariate processes, in applications where a response is influenced by several variables and the objective is to optimise this response. Box and Wilson first introduced the theory of RSM in 1951 [3], and RSM is today the most commonly used method of process optimisation [4]. Using RSM one may model and predict the effect of individual experimental parameters on a defined response output, as well as locating any interactions between the experimental parameters which otherwise may have been overlooked. RSM has been employed extensively in the field of engineering and manufacture [5-11] where many parameters are involved in a process. RSM is now used widely in such diverse fields as microbiology [12,13], pharmacology [14], vehicle crash-testing [15] and food chemistry [16] etc. RSM has been applied to the optimisation of laser welding [17-20] and laser-cutting processes [21], but never before to LIBS hardware optimisation of hardware configuration.

In order to conduct any RSM analysis one must first design the experiment, identify the experimental parameters to adjust, and define the process response to be optimised. Once the experiment has been conducted and the recorded data tabulated, RSM analysis software models the data and attempts to fit a linear or second-order polynomial to this data.

1.3 Optimisation of the RSM experiment

An un-optimised, multi-level full factorial experiment design requires all possible combinations of the experimental parameters to be considered. Increasing the number of parameters and also the number of levels (the variance of each parameter) will increase the number of analyses required as:

$$(\text{no. of levels factor 1}) \times (\text{no. of levels factor 2}) \times \dots (\text{no. of levels factor n}) \quad (1)$$

The software package used in this study was StatGraphics 5.1, which is a highly specified multivariate statistical analysis package. StatGraphics 5.1 provides the capability to optimize a designed experiment. Optimisation of an experimental design reduces the number of experimental runs required to model the response of a system, whilst retaining a comparable level of model accuracy. Algorithmic logic is used to estimate the minimum number of candidate runs required for the optimised design to adequately describe the system under investigation. The data obtained from the candidate runs is analysed in the same manner as in a full experimental design. The fewer candidate runs one conducts, the less accurately the optimised design models the response of the full design. D-optimality is a criterion calculated by the design package and gives a measure of the variability of all the estimated parameters.

2. Experimental set-up

2.1 The LIBS apparatus

The apparatus shown in Figure 2, was designed to be fully flexible and allow the LIBS analysis of solids, liquids and gases through a range of pressure regimes, from atmosphere down to $<10^{-6}$ mbar. The set-up includes a Surelite Continuum Nd:YAG laser, frequency doubled to produce an output at 532 nm, with 4-6 ns pulse length and a peak power of 200 mJ. The laser may be operated at repetition rates of up to 10 Hz, but for this investigation was limited to 1 Hz in order to reduce the gas load on the vacuum pump set. Laser radiation is focussed onto the sample using a 300 mm convex lens that is mounted on a micrometer stage allowing positional adjustment along the axis of the laser beam of 30 mm either side of the focal position.

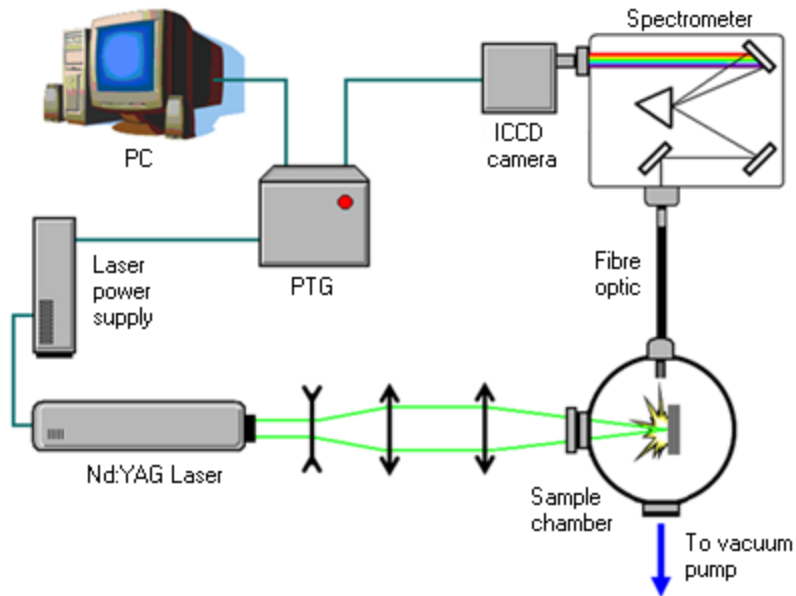


Figure 2. Schematic diagram of the LIBS apparatus.

The sample is mounted in the vacuum chamber on an x-y stage so that each LIBS analysis can be performed away from previous ablation sites. The laser is focussed onto the material under test inside the vacuum chamber through a quartz window mounted in a Con-Flat carrier. A Leybold TurboVac 50 turbomolecular pump backed by a Leybold TriVac rotary pump is used to evacuate the chamber to pressures $<10^{-6}$ mbar. A molecular sieve foreline trap was employed in order to reduce pump oil contamination back-streaming into the chamber.

Optical emission from the plasma plume is collected through a two metre fibre-optic cable, manufactured by Roper Scientific, with a wavelength range of 190 to 1100 nm and a collection angle of 25° . The fibre-optic cable is inserted into the vacuum chamber using a specially designed, elastomer sealed feed-through and is coupled to an Acton Research Spectra Pro 500i 0.5 m imaging triple grating ($150, 600, 2400 \text{ gmm}^{-1}$) spectrometer. The output of the spectrometer is coupled to a Princeton Instruments PI-MAX ICCD camera that utilises a proximity focussed MCP intensifier connected via a fibre-optic coupling to the CCD array. The 1024×256 pixel CCD array is thermoelectrically cooled. A 1 ns increment in the gate delay and width is possible with a

resolution of 40 ps. The laser power supply, camera and PC are connected to a Princeton Instruments ST-133A programmable timing generator, enabling temporal resolution of the plasma plume. Roper Scientific's WinSpec/32 spectrum capture and manipulation software allows both capture of optical emission and identification of any prominent peaks present.

In this work, standard semiconductor grade [111] silicon wafers were analysed. Six silicon I lines in the 250 - 253 nm wavelength range were monitored using the 2400 gmm^{-1} grating. Each data set was an accumulation of ten spectra.

2.2 Analysis software

This study used experiments that were designed and analysed solely with StatGraphics 5.1. In order to simplify the analysis of any multivariate system, one must specify the response that is to be optimised.

The ultimate aim of this study was to identify the parameters that would produce the best possible compromise of peak signal to background noise ratio, related to the peak resolution.

In order to model these two factors as a single system response the Quality Factor (QF) of the LIBS spectra was conceived and defined:

$$QF = \frac{\text{peak height}}{\text{delta background}} \times \frac{0.04}{FWHM} \quad (2)$$

Where: peak height is the maximum peak value minus the average background signal, delta background is the maximum background level minus the minimum background level (i.e. the spread/variance of the background noise), FWHM is the full-width at half-maximum of the measured peak and 0.04 is the minimum FWHM measurable by the instrument in nm. The goal of the investigation was to optimise the QF value for both vacuum and atmospheric conditions.

Table 1. Factors and settings for RSM experiment.

Factor	Setting			
gain	0	50	100	150
slit width (μm)	20	70	120	-
lens position (mm)	-15	0	+15	-
width (ns)	200	466.67	733.33	1000
gate delay (ns)	100	500	900	1300
ambient pressure	1	0	-	-

The parameter settings chosen for this investigation, shown in Table 1, represent the parameter space of the RSM model. Initially a simple first-order screening experiment was conducted with a large parameter space in order to estimate an overall QF response. With the QF response estimated over a broad parameter space, finer parameter settings were then pinpointed.

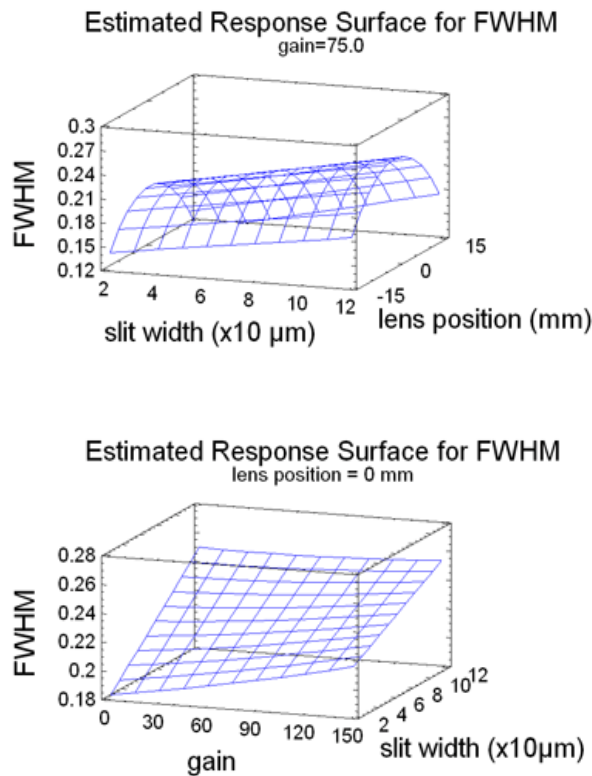
Spectrometer gain, camera gate delay and gate width were deemed to have greater impact on QF and as such set to four levels each for a more thorough investigation. The spectrometer input slit width was varied over three levels, 20, 70 and 120 μm . Three positions of the lens, focussing the laser 15 mm in front of the sample (-15 mm), at the sample surface (0 mm) and 15 mm beneath the surface of the sample (+ 15mm) were also selected.

StatGraphics 5.1 requires that all input parameters have numerical values; atmospheric pressure is signified by 1, vacuum conditions by 0. The finished un-optimised experiment design delivered a proposed 1152 experimental runs. To reduce this number, the experiment design was divided into two. Splitting the design reduces the ability to observe all interactions between all parameters. The parameters judged to have the greatest interactions were grouped together; one experimental design combined lens position, slit width and gain (36 runs), and the second experimental design combined gate delay, gate width and ambient pressure (32 runs). The run order of both designs was randomised to reduce the effect of any lurking variables such as ambient temperature,

humidity, laser power fluctuation etc. Both designed experiments were performed twice to improve accuracy. Initially peak height and FWHM were considered as separate responses before finally being combined into the QF in order to fully describe the response of the LIBS apparatus.

3. Results and discussion

3.1 Estimated response surfaces- FWHM

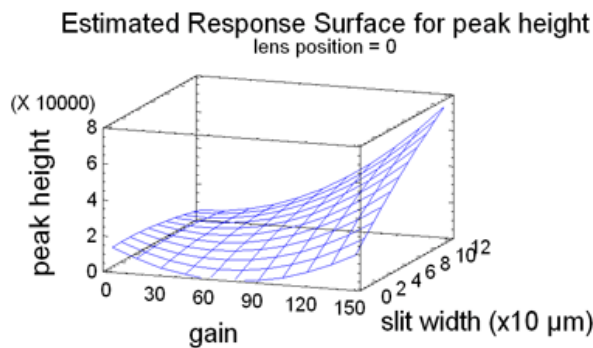
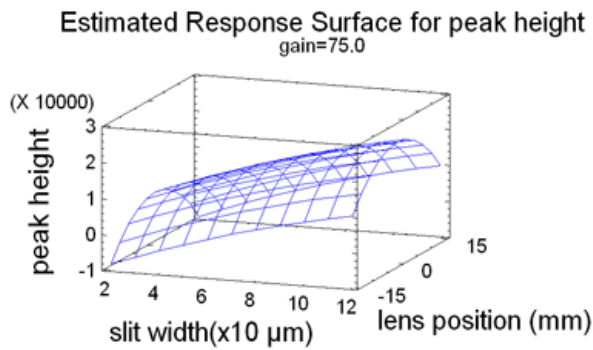


Figures 3a and 3b. Estimated response surfaces for FWHM, varying slit width, lens position and gain at atmospheric pressure.

Figures 3a and 3b show the estimated response surfaces generated for FWHM whilst varying spectrometer input slit width, lens position and gain at atmospheric pressure. Figure 3a shows the predicted effects of varying lens position and slit width at a constant gain of 75; it can be seen that there is a maximum value of FWHM with the lens position focussing the laser at the sample surface, and that FWHM appears to increase linearly with slit width. Figure 3b shows the effects of varying gain and slit width at a constant

lens position of 0 (the focal point); it can be seen that the FWHM increases linearly with both gain and slit width. If the major concern regarding spectra capture is to minimise FWHM, thus improving resolution, then Figures 3a and 3b suggest that LIBS analysis should be conducted at low gain, with small slit width and focussing the laser either in front of or beneath the surface of the sample.

3.2 Estimated response surfaces- peak height



Figures 4a and 4b. Estimated response surfaces for peak height, varying slit width, lens position and gain at atmospheric pressure.

Figures 4a and 4b show the estimated response surfaces generated for peak height whilst varying spectrometer input slit width, lens position and gain at atmospheric pressure. Figure 4a shows the effects of varying lens position and slit width at a constant gain of 75; it can be seen that 0 is the optimal lens position producing maximum peak height, and that peak height increases linearly with slit width. Figure 4b shows the effects of varying gain and slit width at a constant lens position of 0; it can be seen that peak height again

appears to increase linearly with slit width. Peak height appears to vary as a quadratic term with gain. This is not actually the case as the spectrum intensity increases exponentially with gain. The erroneous shape of the estimated response surface is due to the fact that StatGraphics can only fit a second order polynomial to the data set. To verify this exponential trend, the increase of peak height (counts) with gain this was plotted manually for slit widths of 20, 70 and 120 μm , and shown in Figure 5.

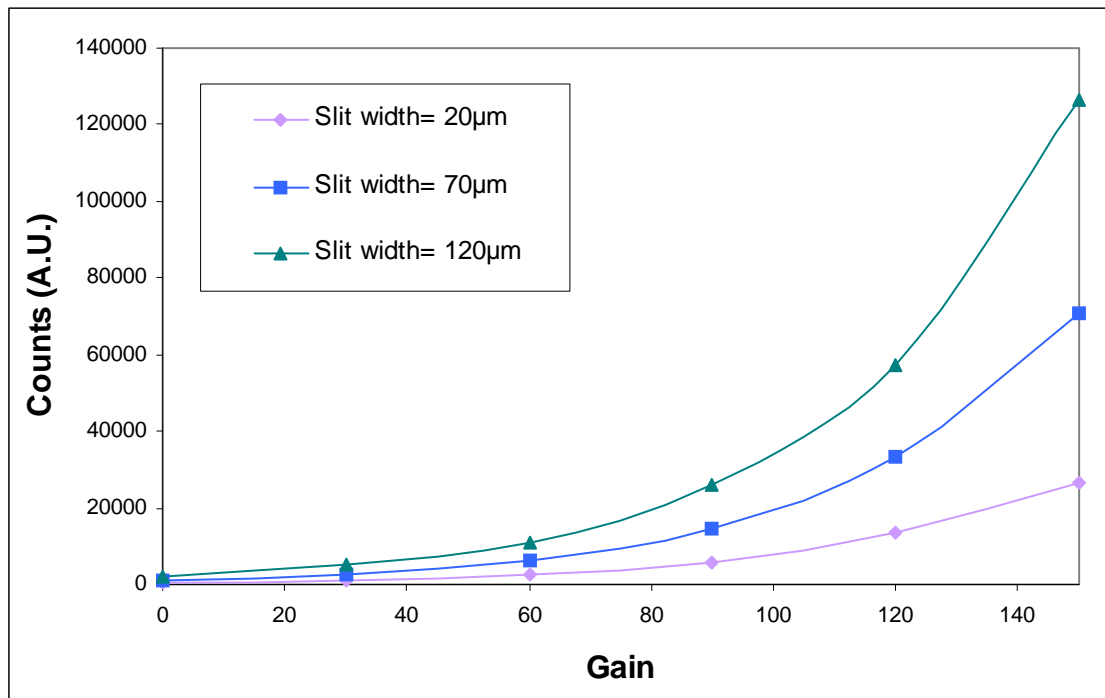
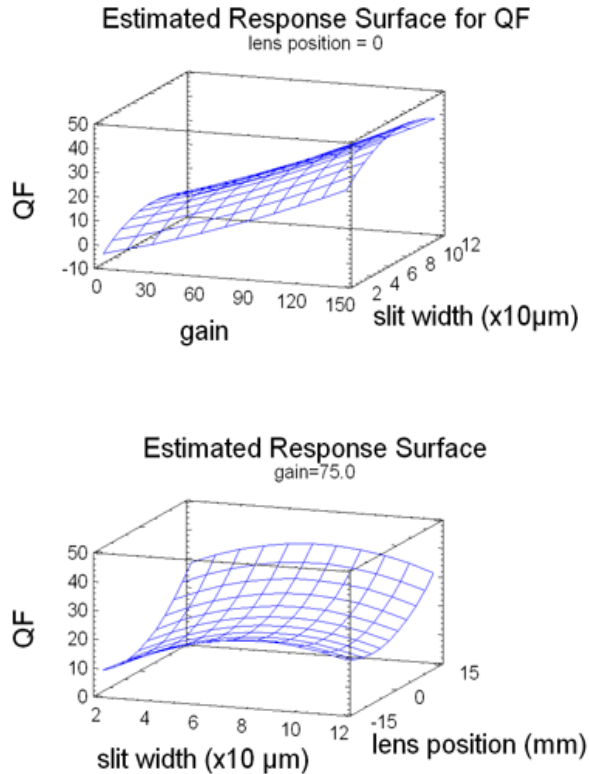


Figure 5. Graph to verify surface plot accuracy.

Each data point in Figure 5 is the average of three readings. An exponential fit to each line has an R-squared value of 0.99; therefore the effect of increasing gain on peak height definitely follows an exponential trend, not a quadratic as shown by StatGraphics. The erroneous shape of the estimated response surface generated in Figure 4b warns caution when analysing surface plots, although it does indicate the general trend of an increase of peak height with gain. Figures 4a and 4b indicate that if the primary concern regarding spectrum capture is to maximise peak height, and therefore sensitivity, then LIBS analyses should be conducted with high gain, a large slit width and the laser focussed at the surface of the target material.

3.3 Estimated response surfaces- QF

The two separate responses of peak height and FWHM were then combined into the single response of QF, as defined in Equation 2.



Figures 6a and 6b. Estimated response surfaces for QF, varying slit width, lens position and gain at atmospheric pressure.

Figures 6a and 6b show the estimated response surfaces generated for QF whilst varying spectrometer input slit width, lens position and spectrometer gain at atmospheric pressure. Figure 6a shows the effect of varying slit width and gain at a constant lens position of 0, indicating that there is an optimum slit width at around 9 μm , and that QF increases linearly with gain. Figure 6b shows the effect of varying slit width and lens position at a constant gain of 75, indicating again an optimum slit width of 9 μm , and also that QF is optimised at the extremes of lens position, +15 mm and -15 mm. According to the StatGraphics model, if one desires to optimise the LIBS hardware to maximise QF at atmospheric pressure, then LIBS analyses should be conducted at high gain, with a slit

width of 9 μm , and by placing the lens at either of its extreme positions.

3.4 Estimated response surface- optimised experiment

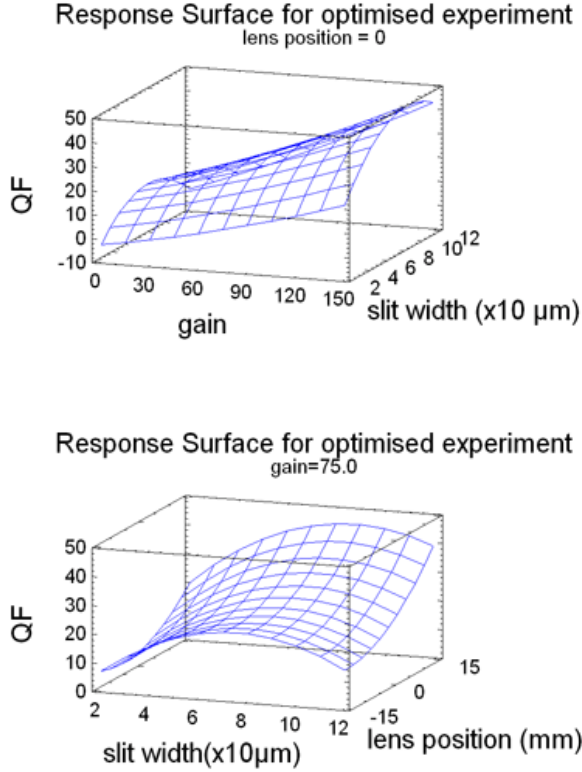


Figure 7. Estimated response surface for optimised experiment for QF, varying slit width, lens position and gain at atmospheric pressure.

To determine how accurately an optimised experimental design represents the full design, experiment 1 (combining slit width, lens position and gain with QF as the output response) was optimised and performed again. The original full design required 36 runs (72 with repeat), the optimised design was reduced to 12 runs with a D-optimality of 48.125%. The estimated response surface generated is shown in Figure 7, which may be compared with that generated from the full design in Figure 6b. It can be seen that although the optimised design estimated response surface does not match exactly that of the full design, the general trend of the QF response is remarkably similar. It appears that optimising an experiment design yields great advantages in terms of the time and effort saved, whilst still maintaining an acceptable level of accuracy in the model.

3.5 Comparison of QF response under vacuum and at atmospheric pressure

The optimisation of a full experiment design for LIBS at atmospheric pressure has been shown to provide an accurate model of the system; consequently experiment 2 was optimised to reduce the number of runs. Further to this, the experiment was augmented to include a more thorough investigation of slit width over four levels. The revised parameter space for experiment 2 is shown in Table 2.

Table 2. Augmented parameter space for experiment 2.

Factor	Setting			
slit width (μm)	8.0	14.0	20.0	26.0
lens position (mm)	-15	0	+15	-
width (ns)	200	466.67	733.33	1000
gate delay (ns)	100	500	900	1300

The augmented full design of experiment 2 required 188 (no repeat) runs and was subsequently optimised to 20 candidate runs with a D-optimality of 44.874%. Experiment 2 was performed at atmospheric pressure and also under vacuum conditions; the estimated response surfaces for QF are shown in Figures 8 and 9 respectively.

Response Surface for QF at atmospheric pressure
slitwidth = 140 μm , lens position = 0

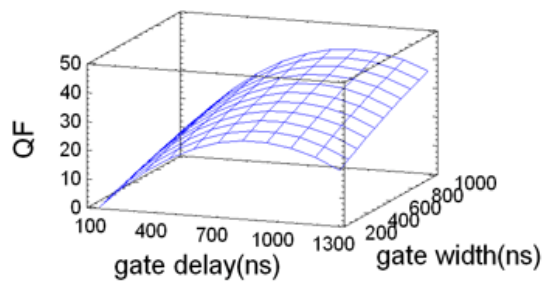


Figure 8. Estimated response surface for QF, varying gate delay, gate width, lens position and slit width-atmospheric pressure.

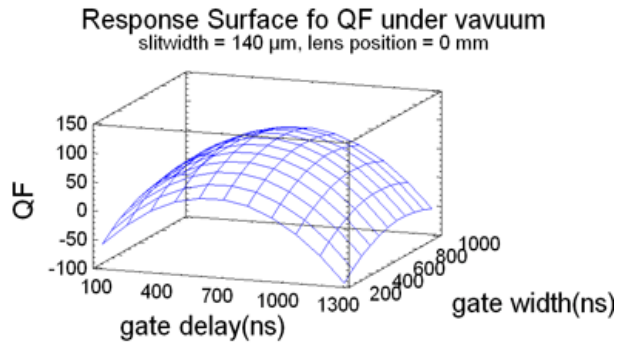


Figure 9. Estimated response surface of QF, varying gate delay, gate width, lens position and slit width- vacuum conditions.

Figures 8 and 9 reveal the difference in the response of QF for LIBS conducted at atmospheric pressure when compared to that obtained under vacuum conditions.

Table 3. Optimised Response: QF at atmospheric pressure.
Optimum QF value = **53.7069**

Factor	Low	High	Optimum
Slit width	2.0	26.0	26.0
Lens position	-15.0	15.0	14.8148
Gate delay	100.0	1300.0	952.953
Gate width	200.0	1000.0	1000.0

Table 4. Optimised Response: QF under vacuum conditions.
Optimum QF value = **262.32**

Factor	Low	High	Optimum
Slit width	2.0	26.0	2.0
Lens position	-15.0	15.0	15.0
Gate delay	100.0	1300.0	576.513
Gate width	200.0	1000.0	745.712

Tables 3 and 4 show the lowest and highest values assigned to each parameter, under

atmospheric pressure and vacuum conditions respectively, used to generate the estimated response surfaces given in figures 8 and 9. The optimum values stated are those that StatGraphics predicts will maximise the QF value. When comparing the two sets of results it can be seen that the only parameter that has the same optimum setting is the lens position. All the other optimum parameter settings reveal a unique set of conditions for atmospheric pressure LIBS compared to those under vacuum for maximised QF. Where the optimum value is equal to the high or low setting then the parameter space may not have been sufficiently large enough to locate the true optimum value.

3.6 Summary of results

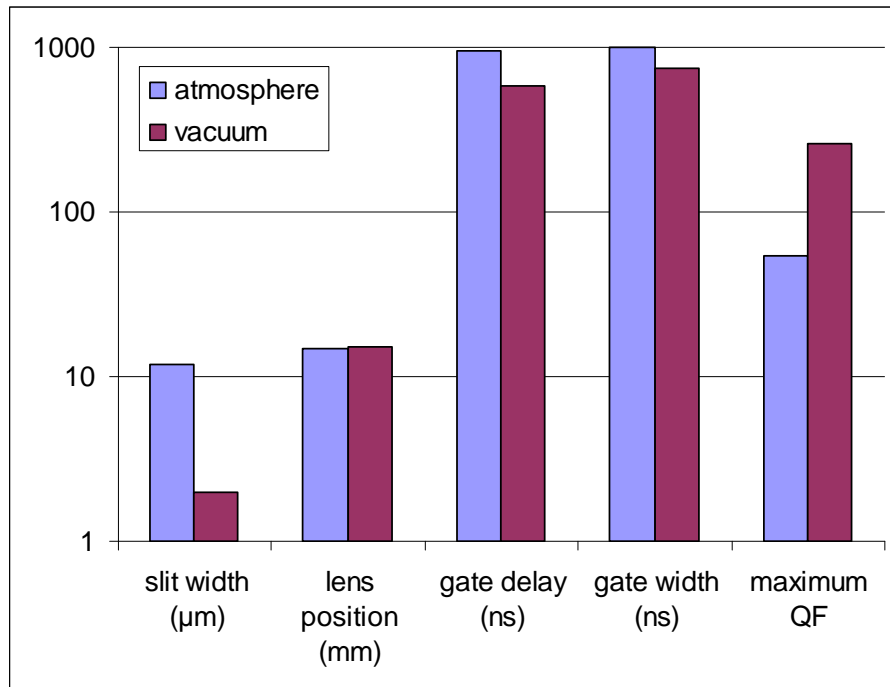


Figure 10. A comparison of the optimum settings for vacuum and atmospheric pressure conditions.

Figure 10 shows the optimum parameter settings for maximising QF, and the maximum value for the QF, at atmospheric pressure and under vacuum conditions as indicated by StatGraphics. The maximum QF value is seen to be much higher for LIBS conducted under vacuum conditions (262.32) than that obtained for atmospheric pressure LIBS (53.7069). Using the definition of QF as given in Equation 2, it is predicted that spectra with the highest sensitivity and resolution should be observed when performing LIBS

under vacuum conditions.

Pareto charts were used to graphically summarize and display the relative importance of each parameter with respect to the overall QF response at both atmospheric pressure and under vacuum conditions. The Pareto charts show all the linear and second order effects of the parameters within the model and estimate the significance of each with respect to maximising the QF response.

The results obtained under atmospheric conditions, shown in Figure 11, predict that there are 4 significant parameters at a 95% confidence level: the linear gate delay; the linear gate width; a negative second order lens position and a linear lens position. These are the major terms in a polynomial fit to the data. The R-Squared statistic indicates that this model as fitted explains 92.7798% of the variability in QF.

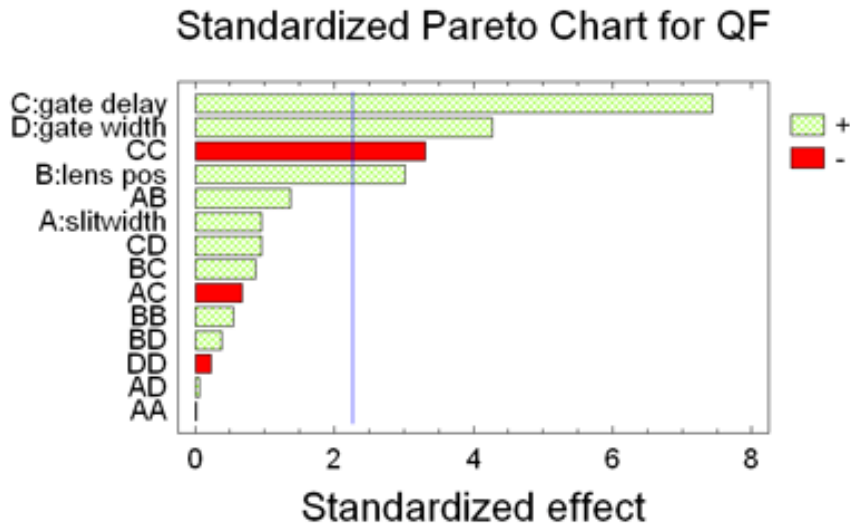


Figure 11. Pareto chart for QF response under atmospheric pressure conditions.

The results obtained under vacuum conditions, shown in Figure 12 predict that there are now only 2 significant parameters with a 95% confidence level: a negative second order gate delay and a negative linear slit width. The R-Squared statistic indicates that this model as fitted explains 81.2335% of the variability in QF.

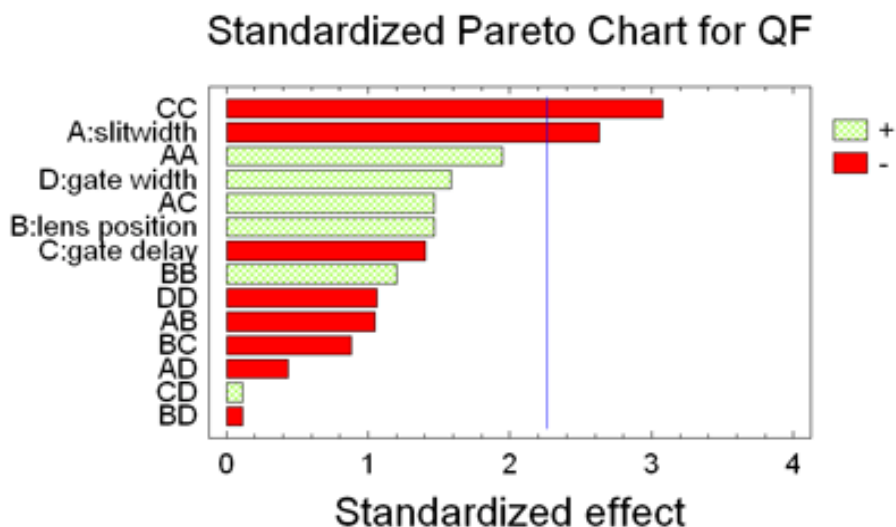


Figure 12. Pareto chart for QF response under vacuum conditions.

4. Conclusion

RSM has been applied to modelling the LIBS system parameters, predicting the response of the system and thus the nature of the output i.e. the resolution and sensitivity of the system. Discrepancies between the RSM model and experimental observations are due to the fact that StatGraphics is only capable of fitting first or second order polynomial models to the data set. As was shown in Figure 5, the data need not necessarily follow either of these models. When peak height as a function of gain was investigated in more detail, it was shown that this followed an exponential fit.

StatGraphics has been used to analyse the LIBS hardware configurations under both atmospheric and vacuum conditions; revealing that there are unique hardware configurations for optimising QF under these two conditions. At atmosphere it has been shown that there are 4 significant experimental parameters, whereas under vacuum conditions only 2 experimental parameters are significant. According to the definition of QF as given in Equation 2, it was predicted by StatGraphics that spectra with the best possible compromise of resolution and sensitivity should be observed when performing LIBS under vacuum conditions. Our experimental work confirms this conclusion [22].

Optimising a designed experiment, thereby reducing the number of runs necessary to

understand all the input parameter interactions, retains a moderate level of model accuracy and should therefore be applied with care when analysing a complex multivariate process. By its nature RSM may never fully describe a system, but may offer an insight into the general trends and any interactions occurring.

Acknowledgements

Special thanks to Wayne Lawson C.Eng for introducing us to the technique of RSM; his advice and encouragement have been most helpful.

References

- [1] C.C Garcia, J.M. Vadillo, S.Palanco, J. Ruiz, J.J. Laserna, Comparative analysis of layered materials using laser-induced plasma spectrometry and laser-ionization time-of-flight mass spectrometry, *Spectrochimica Acta Part B* 56 (2001) 923-931.

- [2] S.S Harilal, C.V. Bhindu, M.s. Tillack, F. Najmabadi, A.C. Gaeris, Internal structure and expansion dynamics of laser ablation plumes into ambient gases, *Journal of Applied Physics*, 93 (2003) 2380-2388.

- [3] G.E.P. Box, K.B Wilson, Experimental attainment of optimum conditions, *Journal of the Royal Statistical Society*, 13 (1951) 1-45.

- [4] D. Bas, I.H. Boyaci, Modeling and optimization I: Usability of response surface methodology, *Journal of Food Engineering*, 78, (2007) 836-845.

- [5] J. Kwak, Application of Taguchi and response surface methodologies for geometric error in surface grinding process, *International Journal of Machine Tools and Manufacture*, 45, (2005) 327-334.

- [6] I. A. Choudhury, M. A. El-Baradie, Machinability assessment of inconel 718 by factorial design of experiment coupled with response surface methodology, *Journal of Materials Processing Technology*, 95 (1999) 30-39.

- [7] N. H. Loh, S. C. Tam, S. Miyazawa, Use of response surface methodology to optimize the finish in ball burnishing, *Precision Engineering*, 12 (1990) 101-105.
- [8] P. Krajnik, J. Kopac, A. Sluga, Design of grinding factors based on response surface methodology, *Journal of Materials Processing Technology*, 162-163 (2005) 629-636.
- [9] M. Y. Noordin, V. C. Venkatesh, S. Sharif, S. Elting, A. Abdullah, Application of response surface methodology in describing the performance of coated carbide tools when turning AISI 1045 steel, *Journal of Materials Processing Technology*, 145 (2004) 46-58.
- [10] G. C. Onwubolu, S. Kumar, Response surface methodology-based approach to CNC drilling operations, *Journal of Materials Processing Technology*, 171 (2006) 41-47.
- [11] L.E. Chávez-Valencia, A. Manzano-Ramírez, G. Luna-Barcenas, E. Alonso-Guzmán, Modelling of the performance of asphalt pavement using response surface methodology, *Building and Environment*, 40 (2005) 1140-1149.
- [12] G. Zurera-Cosano, R.M. García-Gimeno, R. Rodríguez-Pérez, C. Hervás-Martínez, Performance of response surface model for prediction of *Leuconostoc mesenteroides* growth parameters under different experimental conditions, *Food Control*, 17 (2006) 429-438.
- [13] P. Kalathenos, J. Baranyi, J. P. Sutherland, T. A. Roberts, A response surface study on the role of some environmental factors affecting the growth of *Saccharomyces cerevisiae*, *International Journal of Food Microbiology*, 25 (1995) 63-74.
- [14] R. J. Belloto, Jr. , A. M. Dean, M. A. Moustafa, A. M. Molokhia, M. W. Gouda, T. D. Sokoloski, Statistical techniques applied to solubility predictions and

pharmaceutical formulations: an approach to problem solving using mixture response surface methodology, *International Journal of Pharmaceutics*, 23 (1985) 195-207.

[15] J. Forsberg, L. Nilsson, Evaluation of response surface methodologies used in crashworthiness optimization, *International Journal of Impact Engineering*, 32 (2006) 759-777.

[16] C. Liyana-Pathirana, F. Shahidi, Optimization of extraction of phenolic compounds from wheat using response surface methodology, *Food Chemistry*, 93 (2005) 47-56.

[17] A.G. Olabi, G. Casalino, K.Y. Benyounis, M.S.J. Hashmi, An ANN and Taguchi algorithms integrated approach to the optimization of CO₂ laser welding, *Advances in Engineering Software*, 37 (2006) 643-648.

[18] H. Lee, H. Han, K. Son, S. Hong, Optimization of Nd:YAG laser welding parameters for sealing small titanium tube ends, *Materials Science and Engineering: A*, 415 (2006) 149-155.

[19] K.Y. Benyounis, A.G. Olabi, M.S.J. Hashmi, Effect of laser welding parameters on the heat input and weld-bead profile, *Journal of Materials Processing Technology*, 164-165 (2005) 978-985.

[20] L. K. Pan, C.C. Wang, Y. C. Hsiao, K. C. Ho, Optimization of Nd:YAG laser welding onto magnesium alloy via Taguchi analysis, *Optics & Laser Technology*, 37 (2005) 33-42.

[21] J. Mathew, G. L. Goswami, N. Ramakrishnan, N. K. Naik, Parametric studies on pulsed Nd:YAG laser cutting of carbon fibre reinforced plastic composites, *Journal of Materials Processing Technology*, 89-90, (1999) 198-203.

[22] J.S. Cowpe, J.S. Astin, R.D. Pilkington, A.E. Hill, Laser-Induced Breakdown

Spectroscopy and Laser Ablation Mass Spectrometry analysis of silicon: effects of ambient atmosphere. To be published.